Spatially Varying Color Distributions for Interactive Multi-Label Segmentation

Claudia Nieuwenhuis and Daniel Cremers

Abstract—We propose a method for interactive multi-label segmentation which explicitly takes into account the spatial variation of color distributions. To this end, we estimate a joint distribution over color and spatial location using a generalized Parzen density estimator applied to each user scribble. In this way we obtain a likelihood for observing certain color values at a spatial coordinate. This likelihood is then incorporated in a Bayesian MAP estimation approach to multi-region segmentation which in turn is optimized using recently developed convex relaxation techniques. These guarantee global optimality for the two-region case (foreground/background) and solutions of bounded optimality for the multi-region case. We show results on the GrabCut benchmark, the recently published Graz benchmark and on the Berkeley segmentation database, which exceed previous approaches such as GrabCut [32], the Random Walker [15], Santner's approach [35], TV-Seg [39] and interactive graph cuts [4] in accuracy. Our results demonstrate that taking into account the spatial variation of color models leads to drastic improvements for interactive image segmentation.

Index Terms—image segmentation, spatially varying, color distribution, convex optimization

1 Introduction

1.1 Interactive Image Segmentation

Segmentation denotes the task of dividing an image into meaningful, non-overlapping regions. Meaningful, especially in complex images, depends on the user's intention of what he wants to extract from the image. This makes the problem highly ill-posed, so user interaction is indispensable. Typically bounding boxes, contours or scribbles are used to indicate the user's interest. Such interactive segmentation algorithms are widely used in image editing software packages, e.g. for the identification of specific structures in medical images, for tracking objects in a video or to interactively edit and manipulate images. Over the last few years, we have observed a number of breakthroughs in image segmentation regarding algorithmic approaches to efficiently compute minimum energy solutions for respective cost functions, using graph cuts [16], [5], level set methods [11], random walks [15] and convex relaxation techniques [8], [42], [19], [7].

Despite substantial algorithmic advances, state-of-the-art approaches to interactive image segmentation often fail for scenes of complex color variability, where objects have similar colors and may be exposed to difficult lighting conditions. The reason is that existing approaches often do not systematically exploit the spatial location of the user information, and rather model the color variation in a given region with a single space-independent color distribution. Due to the strong overlap of respective color distributions the segmentation process often fails – see Figure 2b. In contrast, if only scribble distance is used for region assignment segmentation fails as well – see Figure 2c. By statistically taking into account the local distribution of the scribbles we obtain spatially varying color distributions which are locally separable and allow for drastic improvements in the segmentation – see Figure 2d.

a) original b) segmentation

Fig. 1. Interactive segmentation result. a) The original image exhibits strongly overlapping foreground and background color distributions due to large lighting variations. b) Explicitly taking into account the spatial dependency of color likelihoods leads to drastic improvements of the segmentation.

To obtain a good segmentation result most algorithms require two important concepts: first, based on the user input each pixel is assigned a value measuring how well it fits to each marked region (data fidelity term); second, the consistency of the segmentation with respect to some prior knowledge is imposed (regularization term), e.g. the object boundary length [33], the number of labels [41], specific inter-class cost functions [19] or label co-occurrence [20]. In this paper, we focus on the data fidelity term and its importance for the segmentation of natural images taken under difficult color and illumination conditions such as those in Figure 1. A preliminary version of this work was presented in [25].

1.2 Previous Data Fidelity Terms

Over the years a variety of data fidelity terms for image segmentation have been proposed. The piecewise constant

• *Claudia Nieuwenhuis and Daniel Cremers are with the Department of Computer Science, Technical University of Munich, Germany. E-mail: {claudia.nieuwenhuis,daniel.cremers}@in.tum.de*

a) original b) color c) location d) combination

Fig. 2. a) Original images with strong lighting variations and reflections. b) Segmentation results based on color similarity only. c) Segmentation results based on scribble distance only (i.e. a length-regularized Voronoi tesselation). d) Segmentation results based on spatial and color information of the scribbles.

Mumford-Shah functional [23], for example, is based on representing the color in each region with the mean color value, thus minimizing the color variance in each segment. Instead of a constant mean color value, foreground and background histograms are estimated by Boykov and Jolly [4]. Unger et al. [39] also estimate color histograms in their TV-Seg framework and make a hard decision for foreground/background by means of a user threshold on the histogram distance. Mixtures of Gaussians are employed to approximate these probability distributions for digital matting by Chuang et al. [9], in the GrabCut segmentation approach by Rother et al. [32] and for automatic segmentation of natural images by Tai et al. [37]. Methods from machine learning are also applied to solve the classification task, e.g. support vector machines [12] or random forests [35].

In general, scribbles contain two kinds of information: color and location. Disregarding either one of these two categories leads to suboptimal results as shown in Figure 2. With appropriate user interaction the distance to a scribble may convey information on region affiliation. Grady proposes to model this aspect with a random walk [15]. Bai et al. [2] estimate foreground and background color likelihoods whose gradients are used to define weighted geodesic distances between each pixel and the user scribbles. Spatial information has also successfully been introduced into kernel density estimators, e.g. in the mean-shift approach [10], in segmentation based on geodesic distances [2] or in motion analysis [24]. In [40], [30], [14], [17] distance based sampling was applied to image matting. To estimate the pixel's alpha value, the minimum difference between the linearly interpolated color from each foreground and background sample and the current pixel's color is sought. In [17] an additional penalty is added for samples at large distances from the current location. In contrast to these approaches, in this paper we estimate a joint probability distribution over color and space from the whole set of samples simultaneously.

In unsupervised segmentation the approaches by Taron et al. [38] and Brox and Cremers [6], possibly the most closely related to ours, are alternating schemes of segmentation and color model estimation. While spatial variation of color distributions often degrades the convergence of such *unsupervised* segmentation methods to suboptimal local minima (the respective color distributions simply adapt to the local context), we show that in *interactive* segmentation – combined with recent convex relaxation techniques – explicitly modeling the spatial context of color information leads to drastic performance improvements with optimal or near-optimal results.

1.3 Statistical Models of Spatial Color Variation

In the interactive segmentation scenario the user scribbles contain information on color and space. By disregarding this spatial information in respective density estimates from user scribbles, purely color based approaches implicitly assume that the color likelihood is independent of the spatial location. In real-world scenarios this is obviously a restrictive assumption, in particular for natural images with varying light conditions, and for multicolored objects that often rely on camouflaging by adopting similar colors as their environment.

Yet, the user scribbles do contain spatial information, albeit in a non-trivial highly correlated form. The aim of this work is to systematically exploit this space-dependency of user scribbles in a Bayesian framework for image segmentation. Experiments confirm that modeling the spatial dependency of color likelihoods comes at no extra cost for the subsequent inference algorithms, preserving the same computation times and optimality guarantees, yet it drastically improves segmentation results.

1.4 Contribution: Bridging the Gap between Distance Based and Color Based Segmentation

The contribution of this paper is to demonstrate the importance of regarding not only the color but also the spatial location and distribution of user scribbles in interactive segmentation. The locations of user scribbles are typically highly correlated (rather than uniformly distributed). We present a strategy to account for this violation of the i.i.d. assumption of samples when estimating kernel densities in the joint space of color and location. The resulting approach bridges the gap between purely color based and purely scribble location based dataterms and, thus, generalizes previous approaches within one framework. More specifically, we will see later on that our approach has two interesting limiting cases:

- In one limit, we obtain a segmentation method using the commonly employed space-independent color likelihood (namely in disregard of spatial information).
- In another limit, we obtain a length-regularized Voronoi tesselation (in disregard of color information).

A user defined parameter balances the influence of color and location information. This leads to strongly improved segmentation results within a statistically sound approach.

The proposed framework allows to segment objects with heavily overlapping color distributions. The approach is formulated as an energy minimization problem, which is solved in a variational framework. The solution is provably optimal for two regions, while for multiple regions it lies within small bounds of about less than 1% from the optimal solution. The proposed approach can be easily parallelized with computation times of 1.5 seconds on average and is thus well suited for interactivity. Extensive experiments on published benchmarks show that taking into account spatial scribble information outperforms previous approaches some of which not only use color but also textural information.

2 A Statistical Framework for Segmentation

In this section, we will derive a Bayesian inference formulation for multi-region segmentation in which space-variant color likelihoods are estimated from a set of user scribbles. One of the challenges we address is that the locations of user scribbles are not i.i.d. distributed but spatially correlated.

2.1 Segmentation as Bayesian Inference

Let $I : \Omega \to \mathbb{R}^d$ denote the input image defined on the domain $\Omega \subset \mathbb{R}^2$. The task of segmenting the image plane into a set of n pairwise disjoint regions Ω_i

$$\Omega = \bigcup_{i=1}^{n} \Omega_i, \quad \Omega_i \cap \Omega_j = \emptyset \ \ \forall i \neq j \tag{1}$$

can be solved by computing a labeling $u : \Omega \to \{1, .., n\}$ indicating which of the n regions each pixel belongs to: $\Omega_i = \{x \big| u(x) = i\}$. In the framework of Bayesian inference, one can compute such a segmentation by maximizing the conditional probability

$$\arg\max_u \mathcal{P}(u \,|\, I) = \arg\max_u \mathcal{P}(I \,|\, u)\ \mathcal{P}(u). \tag{2}$$

Assuming that the colors of all pixels are independent of each other, but – in contrast to previous interactive segmentation approaches – not independent of space, we obtain

$$\mathcal{P}(I \,|\, u) = \left(\prod_{x \in \Omega} \Big(\mathcal{P}(I(x),\, x | \, u) \Big)^{dx} \right), \tag{3}$$

where the exponent dx denotes an infinitesimal volume in $\mathbb{R}^2$ and assures the correct continuum limit. Note how the space-dependency of color likelihoods arises naturally in this formulation. It has commonly been neglected, yet we shall show in this paper that taking into account this spatial variation of color distributions based on scribble locations leads to drastic improvements of the resulting interactive segmentation process. Assuming furthermore that the color probability at location x does not depend on the labeling of other pixels $y \neq x$, the product in (3) can be written as

$$\mathcal{P}(I \,|\, u) = \prod_{i=1}^{n} \prod_{x \in \Omega_i} \Big(\mathcal{P}(I(x),\, x \,|\, u(x) = i) \Big)^{dx}. \tag{4}$$

2.2 Inferring Space-Variant Color Distributions

The expression $\mathcal{P}(I(x),\, x \,|\, u(x) = i)$ in (4) denotes the joint probability for observing a color value I at location x given that x is part of region Ω_i. It can be estimated from the user scribbles as follows. Let

$$S_i := \left\{ \begin{pmatrix} x_{ij} \\ I_{ij} \end{pmatrix},\ j = 1, .., m_i \right\} \tag{5}$$

denote the set of m_i user-labeled pixels x_{ij} and corresponding color values I_{ij} associated with a given region Ω_i. Then we can estimate the joint distribution $\hat{\mathcal{P}}$ on the product space of color and location by means of a kernel density estimator [1], [31] of the form:

$$\hat{\mathcal{P}}(I(x), x \,|\, u(x) = i) = \frac{1}{m_i} \sum_{j=1}^{m_i} k \begin{pmatrix} x - x_{ij} \\ I - I_{ij} \end{pmatrix}, \tag{6}$$

i.e. a sum of normalized kernel functions k centered at each sample point in the product space.

Figure 3 shows an example of a distribution in the joint space of color and spatial coordinate estimated from a set of user scribbles. Commonly, the location of the scribbles

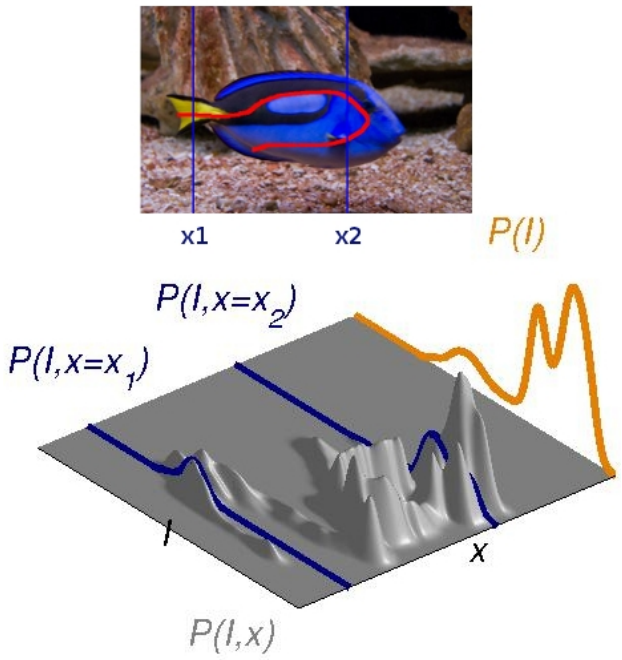

Fig. 3. Above: fish image with user scribbles indicated in red. Below: scribble point based kernel density estimate of the 5-dimensional joint distribution of color and location projected to horizontal location x and grey value I (for readability). If space is not taken into account (i.e. if we marginalize over location) we obtain the same density function $\mathcal{P}(I)$ at each pixel showing several peaks for color values, which are predominant in different parts of the object, like yellow, blue and black. Using the joint distribution gives the probability $\mathcal{P}(I, x)$ for observing a color I at a location x. At each location x we obtain a separate color distribution showing only a single color peak for the locally predominant color, e.g. the yellow color in the fin of the fish at horizontal location x_1 or the darker colors like blue and black in the head of the fish at x_2. The joint 5-dimensional distribution over color and space is used as a dataterm for image segmentation. For challenging real-world images it is drastically more informative than the commonly used space-independent distribution $\mathcal{P}(I)$.

is not taken into account and the space-independent color distribution, the marginal

$$\hat{\mathcal{P}}(I(x) \,|\, u(x) = i) = \int \hat{\mathcal{P}}(I(x), x \,|\, u(x) = i)\, dx, \quad (7)$$

is used, which is plotted on the right. In this case we obtain three peaks, each one for a different predominant color of the foreground object. At each location in the image, the likelihood for each of these colors follows the same marginal distribution, no matter if we are very close to a scribble or far away. In contrast, the proposed distribution allows to distinguish that certain colors may be more or less likely in different locations of the same region Ω_i. Hence, at each location we obtain a separate color distribution depending on the distance to the scribbles. Clearly such relevant information on the spatial variation of a color distribution is entirely lost in the traditional space-independent formulations where the spatial dependency is simply integrated out.

The negative logarithm of the estimated probability distribution can be used as a powerful dataterm for segmentation. For each region Ω_i we obtain the dataterm

$$f_i = -\log \hat{P}(I(x),\, x \,|\, u(x) = i). \quad (8)$$

In practice, we choose Gaussian kernels with widths σ and ρ_i in color and space dimension to define the joint probability distribution

$$\hat{\mathcal{P}}(I(x), x \,|u(x) = i) = \frac{1}{m_i} \sum_{j=1}^{m_i} k_{\rho_i}(x - x_{ij}) k_\sigma(I - I_{ij}). \quad (9)$$

The proposed formulation can be seen as a generalization of the traditional purely color-based approaches. More specifically it has two interesting limiting cases:

- With larger value of ρ_i the influence of the scribble *locations* becomes less important. In the limit $\rho_i \to \infty$ we obtain the purely color-based probability:

$$\hat{\mathcal{P}}(I(x), x \,|u(x) = i) = \frac{1}{m_i} \sum k_\sigma(I - I_{ij}) \quad (10)$$

- With increasing values of σ, the influence of scribble *colors* becomes neglible. In the limit $\sigma \to \infty$ we obtain a purely distance based likelihood:

$$\hat{\mathcal{P}}(I(x), x \,|u(x) = i) = \frac{1}{m_i} \sum k_{\rho_i}(x - x_{ij}) \quad (11)$$

  In the subsequent segmentation process this will lead to a regularized Voronoi tesselation.

Hence, by steering ρ_i and σ, the variance of the kernel density estimators, we can scale the influence of color similarity and scribble distance on the segmentation result.

A variant of the proposed approach can be obtained by using the conditional distribution instead of the joint distribution. The conditional distribution for observing a color I given at coordinate x is obtained by normalizing the joint distribution:

$$\hat{\mathcal{P}}\Big(I(x) \,|\, x, u(x) = i\Big) = \frac{\hat{\mathcal{P}}(I(x), x \,|\, u(x) = i)}{\int \hat{\mathcal{P}}(I(x), x \,|\, u(x) = i)\, dI}. \quad (12)$$

The normalization simply assures that for every point $x \in \Omega$ the probability of observing different colors integrates to 1. Due to the relation

$$P(I, x \,|\, u(x) = i) = P(I \,|\, x, u(x) = i) P(x \,|\, u(x) = i) \quad (13)$$

the joint distribution differs from the conditional by the location prior $P(x \,|\, u(x) = i)$ saying if a specific label is likely in this part of the image. Via this prior the pure scribble distance influences the joint probability distribution leading to Voronoi results in the extreme case as in Figure 2c. In contrast, in the conditional distribution the normalization neglects this location prior leading to a separate color probability distribution at each pixel. In our experiments, both approaches have shown similar results as for small values of σ the location prior does

not have large impact on the dataterm. In this paper, we will concentrate on the joint distribution. This generally gives us more freedom in modeling the dataterm since the influence of location and color can be steered separately by means of α and σ. In contrast, with the conditional distribution (i.e. without location prior) the case of a purely distance based segmentation ($\sigma \to \infty$) cannot be modeled, since we would obtain a constant distribution.

2.3 Handling non-iid Samples

Provided that the samples S are independent and identically distributed (iid), the estimator $\hat{\mathcal{P}}$ in (9) provably converges to the true distribution for $m_i \to \infty$ [36]. Unfortunately, this independence assumption is not fulfilled in practice: while observed color values I_{ij} may be assumed to be independent, the spatial coordinates x_{ij} are certainly not. In particular, the samples are not uniformly distributed in space but given by the scribble pattern. To account for this non-uniformity, we employ spatially adaptive kernel functions by choosing the spatial kernel width $\rho_i(x)$ at location x proportional to the distance from the nearest sample point $x_{v_i} \in S_i$ of region i:

$$\rho_i(x) = \alpha |x - x_{v_i}|_2. \tag{14}$$

The effect of this locally dependent spatial variance is demonstrated in Figure 4. The further away a pixel is from the nearest scribble the more wide-spread becomes the region where scribble points are taken into account for color density estimation at this point. In this way, we obtain locally separable space-variant color distributions as shown in Figure 5.

For several examples, Figure 5b shows samples randomly drawn from the commonly estimated *spatially constant* color distributions of foreground and background. The images are challenging in the sense that the spatially constant distributions strongly overlap making it hard or impossible even for humans to detect the object edges correctly. In contrast, Figure 5c shows randomly drawn samples from *space-variant* color distributions of foreground and background. These reflect the strong variations of color and light in the images. The local adaptation of the probability distributions makes the boundaries of the objects more apparent and ultimately leads to the desired segmentation results, e.g. in Figure 1b.

Figure 6 shows the label probabilities as defined in (9) for different images from the Berkeley and Graz Benchmark.

2.4 Variational Formulation

Having determined the probability distributions $\hat{\mathcal{P}}\big(I, x \,\big|\, u(x) = i\big)$ from the user scribbles for all regions Ω_i, $i = 1, \ldots, n$, we are now ready to solve the optimization problem (2). To this end, we specify the prior $\mathcal{P}(u)$ to favor segmentation regions of shorter boundary:

$$\mathcal{P}(u) \propto \exp\left(-\frac{1}{2}\sum_{i=1}^{n} \mathrm{Per}_g(\Omega_i)\right), \tag{15}$$

where $\mathrm{Per}_g(\Omega_i)$ denotes the perimeter of each set $\Omega_i = \{x \in \Omega \,|\, u(x) = i\}$ measured with either an edge-dependent or a

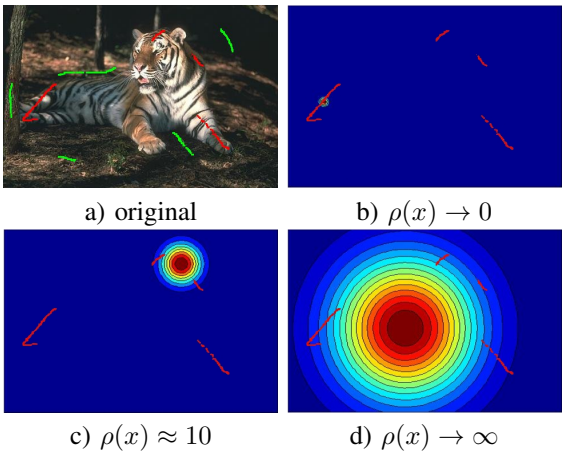

a) original b) $\rho(x) \to 0$ c) $\rho(x) \approx 10$ d) $\rho(x) \to \infty$

Fig. 4. Influence of scribbles (red) for foreground color density estimation at different image locations. b) Close to the scribble $\rho(x)$ tends to 0 and only the closest scribble points influence the color distribution. c) Further away from the scribbles several scribbles in the vicinity influence the estimated color distribution. d) Far away all scribbles have (almost) equal influence on the estimated color distribution similar to the case of spatially constant color models.

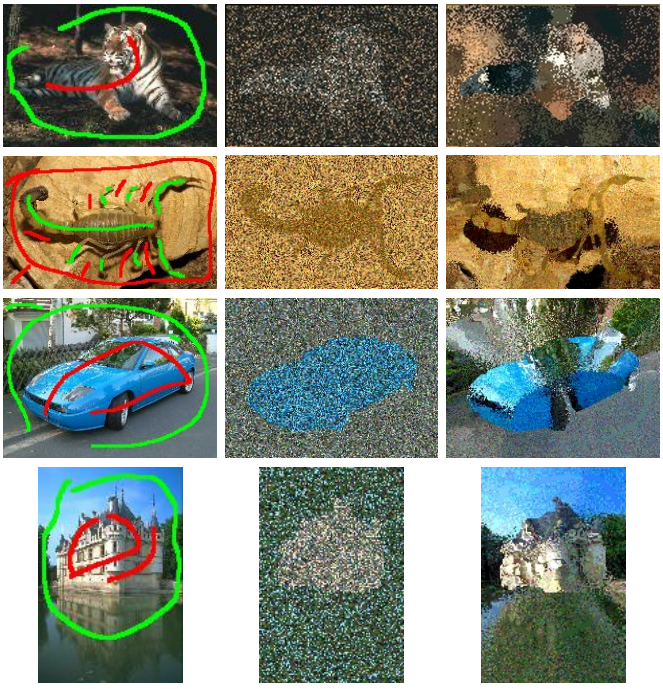

a) original b) spat. constant c) spat. varying

Fig. 5. Random samples from the estimated foreground and background distributions for the tiger image in Figure 1a and others. Neglecting the scribble location (b) makes it hard to distinguish between foreground and background and extract the exact boundary line. If the scribble location is regarded (c) the estimated distributions are locally separable and the synthesized image better approximates the original image colors.

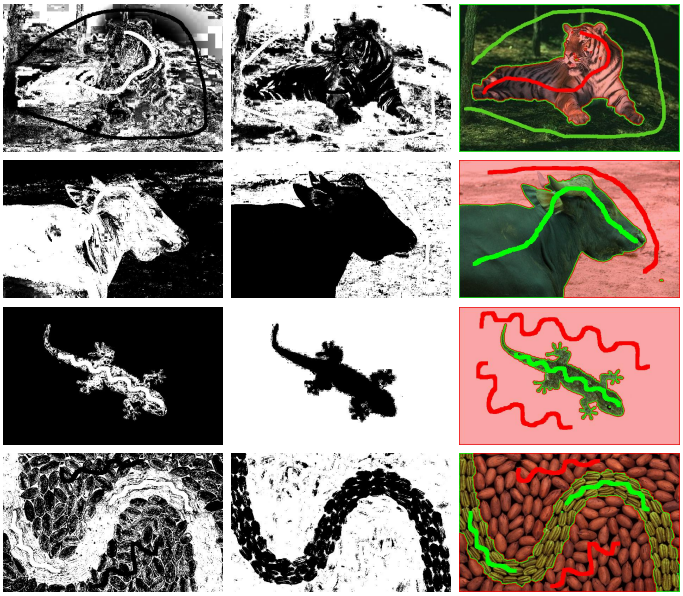

a) foregr. prob. b) backgr. prob. c) segm. result

Fig. 6. Label probability $\hat{P}(I(x), x|\, u(x) = i)$ as defined in (9) for different images from the Berkeley and Graz Benchmark, a) probability for foreground label, b) probability for background label, c) segmentation result

Euclidean metric defined by the non-negative function $g : \Omega \to \mathbb{R}^+$.

$$g(x) = \exp(-\gamma|\nabla I(x)|) \tag{16}$$

for example favors the coincidence of object and image edges. Maximizing the a posteriori distribution (2) can be solved equivalently by minimizing its negative logarithm. Up to constants and according to (15) and (8), the maximum a posteriori estimation is equivalent to the minimization of the energy

$$\begin{aligned} \mathcal{E}(\Omega_1, \ldots, \Omega_n) &= \frac{1}{2}\sum_{i=1}^{n} \mathrm{Per}_g(\Omega_i) + \lambda \sum_{i=1}^{n} \int_{\Omega_i} f_i(x)\, dx, \\ \text{with } f_i(x) &= -\log \hat{\mathcal{P}}\big(I(x)\ x\big|\, u(x) = i\big). \end{aligned} \tag{17}$$

3 Minimization via Convex Relaxation

The optimization problem (17) is a classical shape optimization problem, the continuous equivalent of the Potts model [29], which is known to be NP hard. Building up on recent developments in optimization [8], [42], [19], [7], [27], [18], [28], we solve this problem by means of a convex relaxation strategy with the following favorable properties:

- The segmentation is independent of initialization.
- We obtain globally optimal segmentations for the case of two regions and near-optimal – in practice often globally optimal – solutions for the multi-region case.
- The algorithm can be efficiently implemented on the GPU with average computation times of 0.43 seconds, which makes it suitable for realtime user interactions.

3.1 Conversion to a Convex Differentiable Problem

The key idea is to represent the n regions Ω_i by the indicator function $\theta \in \mathrm{BV}(\Omega, \{0,1\})^n$, where

$$\theta_i(x) = \begin{cases} 1, & \text{if } x \in \Omega_i \\ 0, & \text{otherwise} \end{cases} \qquad \forall i = 1, \ldots, n. \tag{18}$$

Here BV denotes the functions of bounded variation, i.e. functions with a finite total variation. In order to rewrite energy (17) in terms of the indicator functions θ_i, let us observe that the boundary of the set indicated by θ_i can be written by means of the total variation. Let $D\theta_i$ denote the distributional derivative of θ_i (which is $D\,\theta_i = \nabla\theta_i\, dx$ for differentiable θ_i), $\xi_i \in C_c^1(\Omega, \mathbb{R}^2)$ the dual variables with C_c^1 the space of smooth functions with compact support.

Then, following the coarea formula [13] the weighted perimeter of Ω_i is equivalent to the weighted total variation

$$\begin{aligned} \frac{1}{2}\mathrm{Per}_g(\Omega_i) &= \frac{1}{2}\mathrm{Per}_g(\{x\,|\,\theta_i(x) = 1\}) && (19)\\ &= \frac{1}{2} TV_g(\theta_i) && (20)\\ &= \frac{1}{2}\int_\Omega g\, |D\,\theta_i\,| && (21)\\ &= \sup_{\xi_i \in \mathcal{K}_g} \int_\Omega \xi_i\, D\theta_i && (22)\\ &= \sup_{\xi_i \in \mathcal{K}_g} \left(-\int_\Omega \theta_i \ \mathrm{div}\ \xi_i\, dx \right) && (23) \end{aligned}$$

$$\text{with} \quad \mathcal{K}_g = \left\{ \xi_i \in C_c^1(\Omega, \mathbb{R}^2) \,\middle|\, |\xi_i(x)| \le \frac{g(x)}{2}, x \in \Omega \right\}.$$

The latter transformation (23) follows from integration by parts and the compact support of the dual variables ξ_i.

For segmentation, we require that at each location $x \in \Omega$ the sum of all indicator functions amounts to 1, so each pixel is assigned to exactly one label. With this notation, (17) is equivalent to

$$\min_{\theta \in \mathcal{B}} \quad \mathcal{E}(\theta) = \tag{24}$$

$$\min_{\theta \in \mathcal{B}} \sup_{\xi_i \in \mathcal{K}_g} \left\{ \lambda \sum_{i=1}^{n} \int_\Omega \theta_i\, f_i\, dx - \int_\Omega \theta_i \ \mathrm{div}\ \xi_i\, dx \right\} \tag{25}$$

$$\text{with} \quad \mathcal{B} = \left\{ \theta \in \mathrm{BV}(\Omega, \{0,1\})^n \;\middle|\; \sum_{i=1}^{n} \theta_i = 1 \right\}. \tag{26}$$

To obtain a relaxed convex optimization problem which can be minimized globally we relax the set $\mathcal{B}$ to the convex set

$$\tilde{\mathcal{B}} = \left\{ \theta \in \mathrm{BV}(\Omega, [0,1])^n \;\middle|\; \sum_{i=1}^{n} \theta_i = 1 \right\}. \tag{27}$$

3.2 Numerical Implementation

To solve the relaxed convex optimization problem, we employ a primal dual-algorithm proposed in [28]. Essentially it consists of alternating a projected gradient descent in the primal variables θ_i with projected gradient ascent in the dual variables

ξ_i. In addition, it contains an over-relaxation step in the primal variables (giving rise to auxiliary variables $\bar{\theta}_i$):

$$\begin{aligned}
\xi_i^{t+1} &= \Pi_{\mathcal{K}_g}\Big(\xi_i^t + \tau_d \frac{\partial \mathcal{E}}{\partial \xi_i}\Big) = \Pi_{\mathcal{K}_g}\Big(\xi_i^t + \tau_d \nabla \bar{\theta}_i^t\Big) \\
\theta_i^{t+1} &= \Pi_{\tilde{\mathcal{B}}}\Big(\theta_i^t - \tau_p \frac{\partial \mathcal{E}}{\partial \theta_i}\Big) = \Pi_{\tilde{\mathcal{B}}}\Big(\theta_i^t + \tau_p(\text{ div } \xi_i^{t+1} - f_i)\Big) \\
\bar{\theta}_i^{t+1} &= \theta_i^{t+1} + (\theta_i^{t+1} - \theta_i^t) = 2\theta_i^{t+1} - \theta_i^t, \qquad (28)
\end{aligned}$$

where Π denotes the projections onto the respective convex sets and τ_p and τ_d the primal and dual step sizes. The projection onto $\mathcal{K}_g$ is straightforward, the projection onto the simplex $\tilde{\mathcal{B}}$ is given in [22]. As shown in [28], the algorithm (28) provably converges to a minimizer of the relaxed problem for sufficiently small step sizes τ_p and τ_d.

By allowing the primal variables θ_i to take on intermediate values between 0 and 1 we may end up with non-binary solutions. By thresholding these to 0 or 1 we can project solutions back to the binary-valued set $\mathcal{B}$. This projection is known to preserve optimality in case of two regions [8]. In the multi-region case it allows us to compute a bound of optimality given by the energy difference between the minimizer of the relaxed problem and its thresholded version (see Proposition 1). Typically the thresholded solution deviates less than 1% from the optimal energy in the multi-region case.

Proposition 1. *Let $\theta^* \in \mathcal{B}$ be the global minimizer of the original problem (25), $\tilde{\theta} \in \tilde{\mathcal{B}}$ the result of the proposed algorithm for the relaxed problem and $\theta' \in \mathcal{B}$ the binarized solution. Then we can compute an energy bound $\delta(\theta', \tilde{\theta})$ such that the following holds for the energy gap: $E(\theta') - E(\theta^*) \leq \delta(\theta', \tilde{\theta})$.*

Proof: Since $\mathcal{B} \subset \tilde{\mathcal{B}}$, we have $E(\tilde{\theta}) \leq E(\theta^*) \leq E(\theta')$. Energetically the (unknown) optimal binary solution θ^* lies in between the computed relaxed solution $\tilde{\theta}$ and the computed thresholded solution θ':

$$E(\theta') - E(\theta^*) \leq E(\theta') - E(\tilde{\theta}) =: \delta(\theta', \tilde{\theta}).$$

□

3.3 Convergence Analysis

In [28] it has been shown that the presented algorithm converges for $\tau_p \tau_d L^2 < 1$ where L denotes the operator norm of the gradient of θ. To examine the convergence rate, we can compute the primal-dual gap, which is the difference between the primal and the dual energy of the optimization problem. The primal energy is given as the original optimization problem

$$E_p(\theta) = \left\{ \sum_{i=1}^{n} \int_\Omega \lambda\, \theta_i\, f_i\, dx - g(x)\, |D\, \theta_i| \right\} + \delta_{\mathcal{B}}(\theta), \quad (29)$$

where $\delta_{\mathcal{B}}$ is the indicator function of $\mathcal{B}$:

$$\delta_{\mathcal{B}}(\theta) = \begin{cases} 0, & \theta \in \mathcal{B} \\ \infty, & \theta \notin \mathcal{B}. \end{cases} \quad (30)$$

The computation of the dual energy amounts to a point-wise optimization problem

$$\begin{aligned}
E_d(\xi) &= \min_{\theta \in \mathcal{B}} \left\{ \sum_{i=1}^{n} \int_\Omega \lambda\, \theta_i\, (\, f_i - \text{ div } \xi_i)\, dx - \delta_{\mathcal{K}_g}(\xi) \right\} \\
&= \int_\Omega \min_i (f_i - \lambda \text{ div } \xi_i)\, dx - \sum_{i=1}^{n} \delta_{\mathcal{K}_g}(\xi_i). \qquad (31)
\end{aligned}$$

Here $\delta_{\mathcal{K}_g}$ denotes the indicator function for the set $\mathcal{K}_g$. During the optimization, the primal energy constantly decreases, whereas the dual energy increases. When the optimal solution is reached, the primal-dual gap goes to zero. The size of the gap can be used to formulate suitable convergence criteria for the algorithm, e.g. the iterations are terminated if the current gap decreases less than 1% compared to the previous gap. Figure 7 shows the primal-dual gap for up to 2500 iterations for two examples.

4 Results

We have developed an interactive approach for extracting multiple objects from an image. A key contribution of this paper is to regard both color similarity and the local information of the scribbles. To this end, we introduce space-variant color distributions to model objects with spatially varying appearance in the scene. In the following, we will show experimental results on a variety of real-world images and focus on showing how modeling the spatial variation of color distributions leads to substantial improvements of the segmentation over the traditionally employed spatially constant color distributions. We use the following parameters for space-variant color distributions: $\sigma = 1.3$, $\lambda = 0.008$, $\gamma = 5$, $\alpha = 1.8$. $\tau_p = 0.25$ and $\tau_d = 0.5$ according to [26]. To obtain the spatially constant approach we set α to a very large value yielding an (approximately) constant spatial distribution.

4.1 Qualitative Benchmark Results

For automatic segmentation several benchmarks are available, e.g. the Berkeley database, the GrabCut database or the PascalVocDatabase. As extensively discussed in [34], these benchmarks are not suited for testing interactive segmentation. Hence, Santner et al. [35] published a benchmark for interactive scribble based segmentation, the Graz benchmark. We nevertheless start our evaluation on the somewhat simpler trimap segmentation problem of the GrabCut benchmark. In a second step we then evaluate the proposed algorithm on the Graz Benchmark. We also compare against common segmentation algorithms such as GrabCut and Random Walker.

4.1.1 GrabCut Benchmark

For the GrabCut benchmark either bounding boxes enclosing foreground and - inevitably - part of the background can be used as input or trimaps. Since our approach is based on adaptable color distributions rough bounding boxes containing both regions are unsuitable for estimating the probability density functions for foreground and background . Hence, we use the trimap input. Trimaps are maps which roughly segment

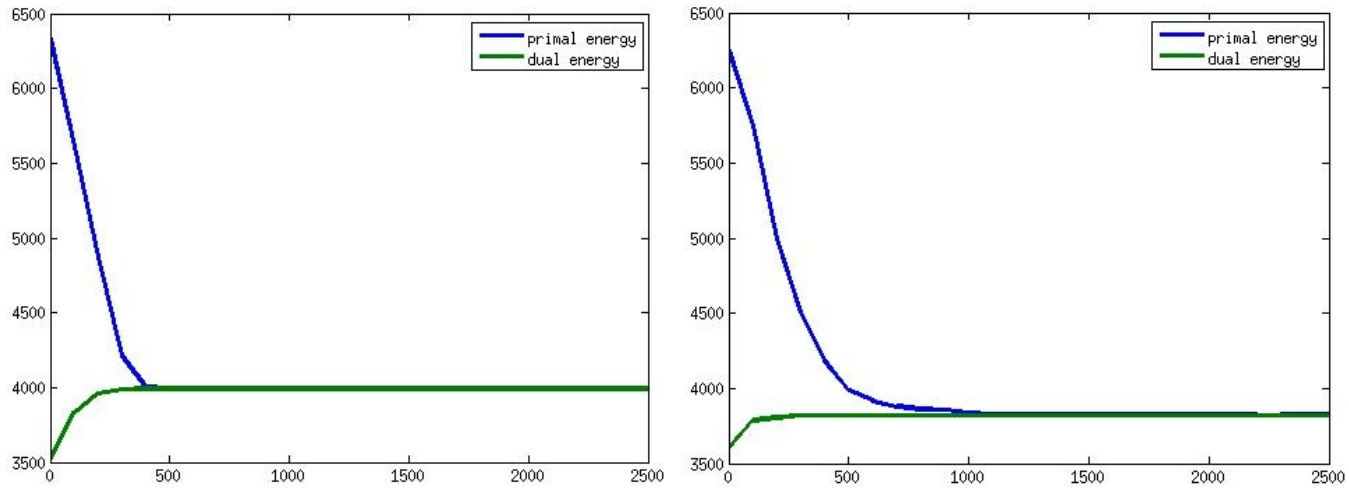

Fig. 7. Convergence analysis of the algorithm for two examples from the Graz Benchmark database. The progress of the primal energy (blue) is depicted with respect to the dual energy (green). The optimal solution of the optimization problem is obtained as soon as the primal-dual gap goes to zero.

the image except the region around the object boundary, which is to be inferred by the algorithm. The benchmark's suitability for testing multi-label segmenation algorithms is limited due to three reasons:

- All examples are limited to two regions, i.e. foreground/background segmentation which means $n = 2$.
- The objects are assumed to be connected.
- The trimaps contain very large seed regions for foreground and background, which already indicate the groundtruth segmentation of most pixels in the image.

Hence, this benchmark simulates strongly simplified conditions for interactive segmentation.

Figure 8 shows several segmentation results from the GrabCut benchmark, the original image on the left, the trimap in the center and the segmentation result on the right. The segmentation results are very close to the groundtruth. Small errors occur due to non-sharp object boundaries (banana), the length regularization (the ear of the llama) or insufficient foreground seed marking (the shoes of the woman).

4.1.2 Graz Benchmark

Since common segmentation databases are not suitable for testing interactive multi-label segmentation [34], Santner et al. recently published the first benchmark for interactive scribble based multi-label segmentation containing 262 seed-groundtruth pairs from 158 natural images containing between 2 and 13 user labeled segments. Santner et al. [35] show impressive results for different combinations of color and texture features: RGB, HSV and CIELab colors combined with image patches, Haralick features and Local Binary Patterns (LBP). However, they neglect the locality of the scribbles by estimating a single, invariant color model for each region. In our experiments we tested the proposed approach with spatially constant and spatially varying color models on their benchmark. If we use the spatially constant model the results are slightly better than those obtained by Santner et al. (RGB color information without texture). They obtain the best results combining CIELab and LBP features in a 21 dimensional vector based on a scribble brush of radius 13. Without reverting to such a sophisticated high-dimensional texture feature space, we obtain a better benchmark performance simply by correctly modeling the spatial variation of color distributions as proposed in this paper.

Figure 11 shows qualitative benchmark results. The figure contains 16 image pairs, where we contrast Santner's best results (CIELab colors combined with LBP features) with the results of our space-variant approach. The locality of the color models allows us to release the regularizing model assumptions, since we can better distinguish between different regions, especially in case of overlapping color models. In this way, for example the second foot of the duck, the fin of the fish, the head of the man at the lake, the legs of the beacon, the oversmoothed contour of the parrot, the astronaut and the feathers of the small bird could be correctly recovered. In case of the snake the locality of the color model helps to assign the objects to the closer matching segment. This explains the higher accuracy of our approach.

Figure 9a shows two examples for failed segmentations, which are due to sparse scribbling. The scorpion image would require more scribbles to adequately model the changing color of the animal. In the second image the red background scribble does not reflect the color change in the upper left image corner. This part of the image is assigned to the foreground due to the strong color similarity with the bee. In Figure 9b scribbles have been added to better reflect the color variance of the scorpion and the background of the bee. Based on this additional information the color distributions are better adapted to the color variation in the images and correct segmentation results can be obtained.

a) Image b) Trimap c) Segmentation

Fig. 8. Results on the GrabCut Benchmark. a) Original image, b) Trimap input (white: foreground, black and dark grey: background, light grey: region to be classified) , c) Segmentation result of the proposed approach.

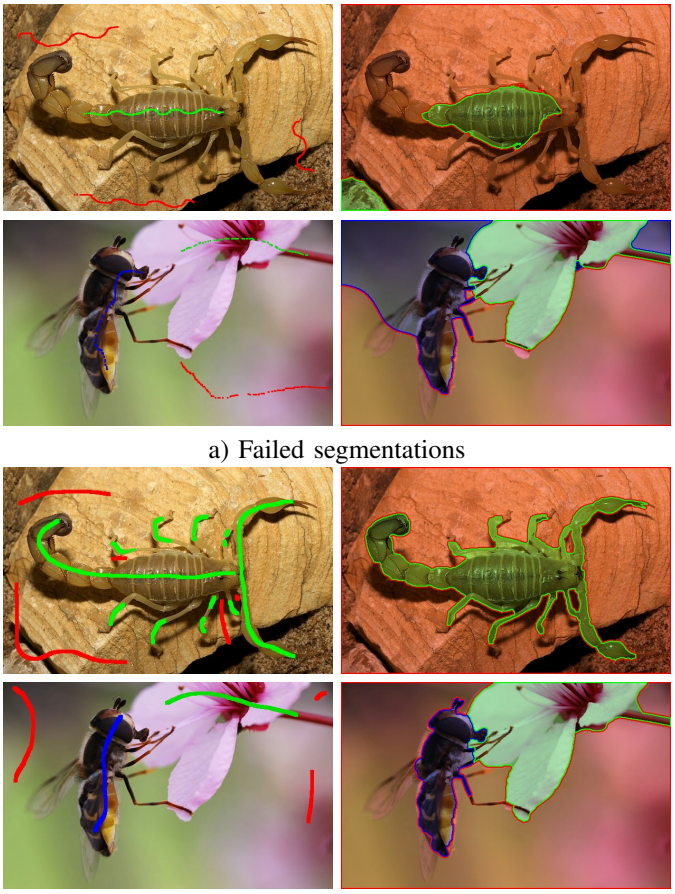

a) Failed segmentations

b) Improved segmentations

Fig. 9. Failed and improved segmentations. a) The scribbles are too sparse to adequately reflect the changing colors in the segments. b) More scribbles have been introduced to obtain the correct segmentations.

4.2 Quantitative Benchmark Results

We now compare the average quality of the proposed algorithm to previous approaches on the GrabCut and the Graz benchmarks. For each benchmark, different quality measures have been published, which will be explained below.

4.2.1 GrabCut Benchmark

Based on the simplified segmentation problem on the GrabCut benchmark, we obtain the results given in Figure 10, which indicates the average misclassification error

$$E_{miss} = \frac{\text{no. of misclassified pixels}}{\text{no. of pixels in unclassified trimap region}}. \quad (32)$$

From the results we can conclude that the proposed approach outperforms the GrabCut approach [3] by 1.4 %. However, the Random Walker approach [15] outperforms both algorithms by far. For the Random Walker we chose $\beta = 100$.

4.2.2 Graz Benchmark

To further assess the quality of the proposed algorithm we apply it to the Graz benchmark dataset containing 262 images with user scribbles. To evaluate the overall segmentation

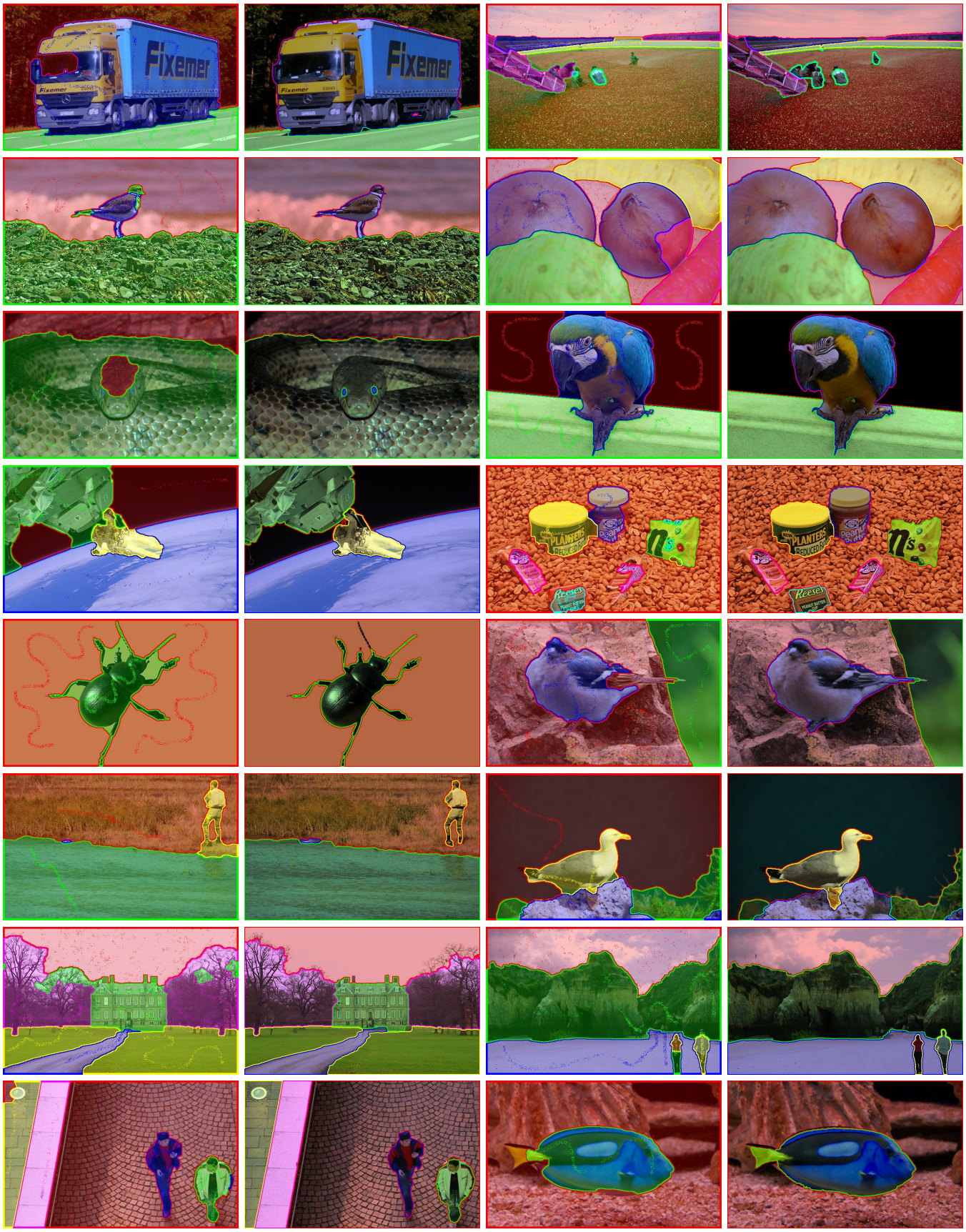

a) Santner et al. b) our approach a) Santner et al. b) our approach

Fig. 11. Results on the Graz benchmark. a) Approach by Santner et al. [35] based on color and texture, b) Proposed space-variant approach regarding scribble locations.

Method	E_{miss} in $\%$
GrabCut - Simple Mixture Model [3]	16.3
GrabCut - learned GMMRF [3]	7.9
our approach, space-variant	6.5
Random Walker [15]	1.1

Fig. 10. Comparison to common segmentation approaches such as the Random Walker approach and the GrabCut approach on the standard GrabCut Benchmark based on the misclassification error (in $\%$) and given trimaps. Segmentation based on trimaps actually represents a simplified problem since the number of objects and the rough boundary are already given. The proposed approach outperforms both variants of GrabCut. The Random Walker shows the best performance.

accuracy Santner et al. [35] compute the arithmetic mean of the Dice-score over all segments. It relates the overlap area of the groundtruth segment $\bar{\Omega}_i$ and the computed segment $\Omega_i = \{x|u(x) = i\}$ to the sum of their areas

$$dice(\bar{\Omega}_i, \Omega_i) = \frac{2|\bar{\Omega}_i \cap \Omega_i|}{|\bar{\Omega}_i| + |\Omega_i|}. \tag{33}$$

Figure 12 compares the average Dice-score of the proposed method to the approach by Santner et al. [35] and the Random Walker [15]. The dimension of the feature vector and the brush size for the scribbles is given. The results indicate that merely regarding the spatial location of scribbles provides stronger performance improvements than a multitude of sophisticated features. Contrary to the GrabCut benchmark, in the more realistic setting posed by the Graz Benchmark, where only small seeds farther away from the object boundary are given, the Random Walker yields the least accurate results of all algorithms.

4.3 Comparison to Foreground Extraction Tools

Most algorithms for interactive segmentation are limited to two regions, i.e. foreground/background extraction. In this section we compare our results to those obtained by TV-Seg [39] and Interactive Graph Cuts [4] for images containing only one object in front of the background. Beyond a quantitative analysis of the performance we examined the qualitative performance with varying amounts of scribbles. To demonstrate the effectiveness of space-variant color models we choose images from the Berkeley database with difficult lighting conditions, reflections or overlapping color models. We used the available implementation of TV-Seg from the TU Graz and the Interactive Graph Cuts implementation in the Toolbox by McGuinness [21]. During segmentation of these images we aimed at minimizing the amount of user scribbles. Figure 13 shows that all three methods provide segmentations of similar quality. However, the proposed space-variant method better reflects the color variations and thus requires fewer scribbles and user interaction.

Method	Dim	Brush	Score
Random Walker [15]	3	13	0.855
Santner et al. [35], RGB	3	-	0.877
our approach, spatially constant	3	3	0.889
[35], CIELab + LBP	21	5	0.917
our approach, space-variant	5	5	0.922
[35], CIELab + LBP	21	13	0.927
our approach, space-variant	5	13	0.931

Fig. 12. Comparison to the multi-label segmentation approach by Santner et al. [35] on the Graz benchmark. For each method the dimensionality of the feature vector, the scribble brush radius and the average dice score are compared. Rather than reverting to sophisticated high-dimensional feature spaces the introduction of spatial information into the estimated color distributions yields better results and allows for higher speeds.

4.4 Multi-Label Segmentation Results

Finally we show results for the spatially constant compared to the spatially varying approach for a collection of interesting images from the Berkeley and Graz database in Figure 14. The first two rows show different animals in front of a similarly colored background. Segmentation here only succeeds based on color and spatial information. The third row shows the displayed goods of a vegetable stall and a skyscraper. In the vegetable stall, the peppers as well as the cauliflower and broccoli exhibit different colors, but belong to the same segment. Since the color distributions of different segments vary and overlap it is important to regard the local distribution of the scribbles to obtain a correct segmentation. The right hand side shows a skyscraper with reflecting windows. Since reflections contain any color from the surroundings, segmentation with global color models is difficult. Based on locally adaptive color models we obtain correct results.

4.5 Runtimes

Interactive image segmentation algorithms demand runtimes close to real-time to be useful for the user. We computed the results on an INTEL XEON 2.27 GHz CPU with an NVIDIA Geforce GTX 580 GPU. The average computation time per image on this benchmark is 1.14 seconds for the dataterm and 0.43 seconds for the optimization for 2 to 13 labels.

4.6 Sensitivity to Parameters and Scribbles

Finally, we examine the sensitivity of the algorithm with respect to parameter choices and scribble locations.

4.6.1 Parameter Sensitivity

The proposed approach requires the user to select four input parameters: the color kernel variance σ, the distance factor

Fig. 14. Multi-label segmentation results for difficult images from the Berkeley and Graz database. The spatially constant approach (b) is compared to the space-variant (c). If spatial scribble information is included in the color model the animals, vegetables and window reflections can be segmented correctly.

α determining the spatial scribble influence, the smoothness factor λ regulating the strength of the dataterm and the parameter γ of the edge indicator function g.

As mentioned above, all experiments reported so far were carried out with a fixed set of parameters. Nevertheless, in order to assess the sensitivity of our algorithm to variations in these parameters we reran the Graz benchmark performance for a variety of parameter settings. Figure 15 shows that for variations of these parameters within a reasonable range, the benchmark performance only varies within 2%. Among the parameters to be set the spatial influence of the scribbles α, the dataterm weight λ and the brush size seem to have the largest impact on the results.

4.6.2 Sensitivity to Scribble Location

Figure 16 shows segmentation results for different amounts and locations of user scribbles. The segmentation based on the first four input sets is almost identical. The random distribution of scribble points in the last image yields slightly better results for the legs of the animal and the stem of the flower due to the wide-spread sample distribution in the image. We can conclude that provided the scribbles are set reasonably to represent the color distributions of the separate regions the segmentation quality is not very sensitive to their amount or location.

5 Conclusion

In this paper we proposed an algorithm for interactive multi-region segmentation which takes into account not only color similarity but also the spatial location of the user scribbles. Since correct density estimation requires iid-assumptions on the spatial location of the scribbles, which is not the case, we proposed a way to handle this problem. The result is a scalable dataterm, which bridges the gap between purely color based and purely distance based segmentations. In this way, overlapping color distributions become locally separable allowing for weaker regularization assumptions and correct segmentations in difficult images. The variational approach is derived rigorously in a framework of Bayesian inference and minimized by efficient convex relaxation techniques, leading to globally optimal solutions for the two-region case and solutions of bounded optimality (and in practice often optimal

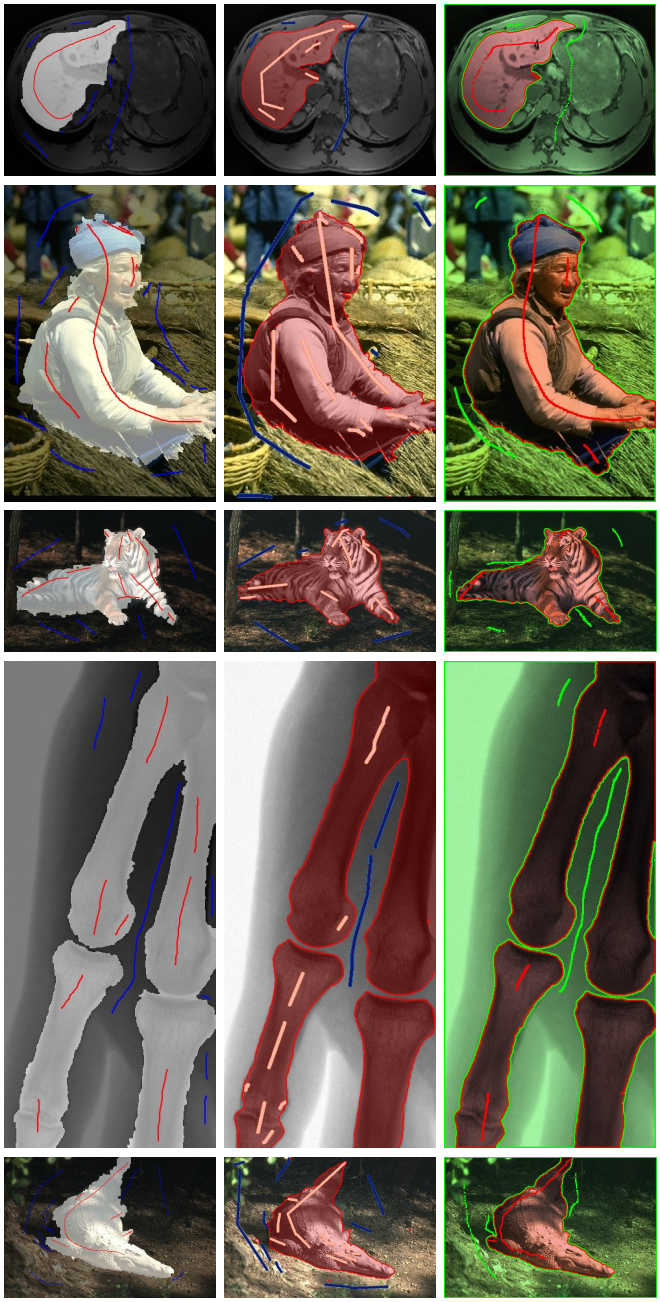

a) Graph Cuts b) TV-Seg c) our approach

Fig. 13. Comparison to known foreground/background extraction approaches. a) Interactive Graph Cuts [4], b) TV-Seg [39], c) proposed space-variant approach. For a) and b) a lot more user interaction is required.

solutions) for the multi-region case. The approach can be parallelized leading to computation times around 1.1 seconds on average for 2 to 13 labels. Results on the GrabCut, Graz and Berkeley databases show that we exceed previous approaches such as GrabCut, Random Walker and TV-Seg.

6 Acknowledgements

We thank Andrew Delong for fruitful discussions of the relations between color-based and space-based distances.

σ	λ	γ	α	Brush	Score
1	100	5	0.7	3	0.909
1.5	100	5	0.7	3	0.909
1.5	100	5	0.7	5	0.910
1.5	100	5	1	5	0.917
1.5	100	4	1	5	0.917
1.5	100	5	1.8	5	0.923
1.5	100	5	1.8	13	0.927
1.3	200	5	1.8	13	0.912
1.3	125	5	1.8	13	0.931

Fig. 15. Sensitivity to parameter modifications. The table shows the average Dice-score on the Graz Benchmark for different sets of the algorithm's parameters. For reasonable choices the performance only varies within 2%.

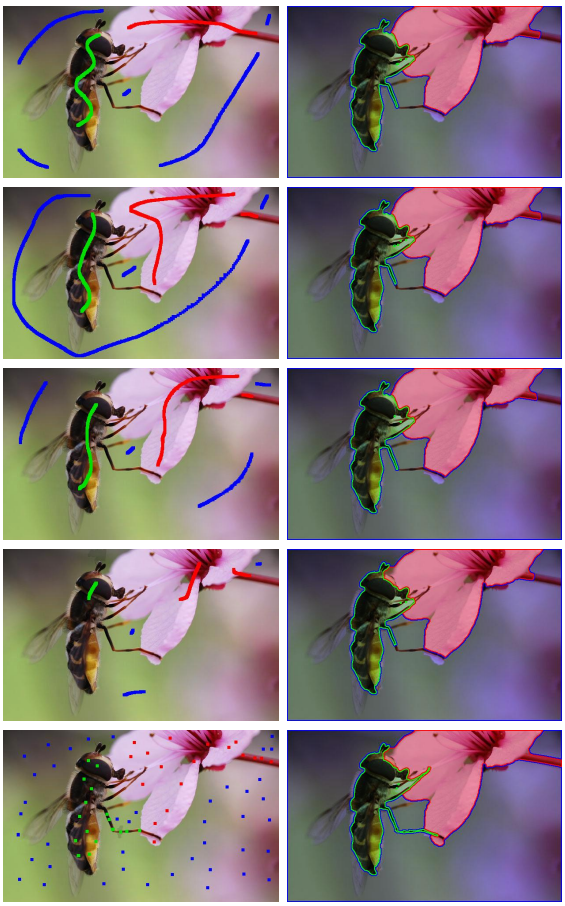

Fig. 16. Segmentation results for different scribble amounts and locations. The results show that the algorithm is not very sensitive to the user input provided that the scribbles are placed in reasonable locations to well represent the color variation in the image.

REFERENCES

[1] H. Akaike. An approximation to the density function. *Ann. Inst. Statist. Math.*, 6:127–132, 1954.

[2] X. Bai and G. Sapiro. A geodesic framework for fast interactive image and video segmentation and matting. In *Proceedings of the International Conference on Computer Vision (ICCV)*, 2007.

[3] A. Blake, C. Rother, M. Brown, P. Perez, and P. Torr. Interactive image segmentation using an adaptive gmmrf model. In *Europ. Conf. on Computer Vision*, 2004.

[4] Y. Boykov and M. Jolly. Interactive graph cuts for optimal boundary and region segmentation of objects in n-d images. In *Proceed. of the Internat. Conference on Computer Vision (ICCV)*, 2001.

[5] Y. Boykov, O. Veksler, and R. Zabih. Fast approximate energy minimization via graph cuts. *IEEE Trans. on Patt. Anal. and Mach. Intell.*, 23(11):1222–1239, 2001.

[6] T. Brox and D. Cremers. On local region models and a statistical interpretation of the piecewise smooth Mumford-Shah functional. *International Journal of Computer Vision*, 84:184–193, 2009.

[7] A. Chambolle, D. Cremers, and T. Pock. A convex approach for computing minimal partitions. Technical report, TR-2008-05, Dept. of Computer Science, University of Bonn, Germany, 2008.

[8] T. Chan, S. Esedoḡlu, and M. Nikolova. Algorithms for finding global minimizers of image segmentation and denoising models. *SIAM Journal on Applied Mathematics*, 66(5):1632–1648, 2006.

[9] Y.-Y. Chuang, B. Curless, D. H. Salesin, and R. Szeliski. A Bayesian approach to digital matting. In *Proceedings of IEEE CVPR 2001*, volume 2, pages 264–271, 2001.

[10] D. Comaniciu and P. Meer. Mean shift: a robust approach to feature space analysis. *IEEE Transactions on Pattern Analysis and Machine Intelligence*, 24:603–619, 2002.

[11] D. Cremers, M. Rousson, and R. Deriche. A review of statistical approaches to level set segmentation: integrating color, texture, motion and shape. *Int. J. of Computer Vision*, 72(2):195–215, April 2007.

[12] O. Duchenne and J.-Y. Audibert. Fast interactive segmentation using color and textural information. Technical report, Certis, Paris Tech., 2006.

[13] H. Federer. *Geometric Measure Theory*. Springer, 1996.

[14] E. S. L. Gastal and M. M. Oliveira. Shared sampling for real-time alpha matting. *Proceedings of Eurographics, Computer Graphics Forum*, 29(2):575–584, 2010.

[15] L. Grady. Random walks for image segmentation. *IEEE Trans. on Pattern Analysis and Machine Intelligence*, 28(11):1768–1783, 2006.

[16] D. M. Greig, B. T. Porteous, and A. H. Seheult. Exact maximum *a posteriori* estimation for binary images. *J. Roy. Statist. Soc., Ser. B.*, 51(2):271–279, 1989.

[17] K. He, C. Rhemann, C. Rother, X. Tang, and J. Sun. A global sampling method for alpha matting. In *Computer Vision and Pattern Recognition*, pages 2049–2056, 2011.

[18] J. Lellmann, F. Becker, and C. Schnörr. Convex optimization for multi-class image labeling with a novel family of total variation based regularizers. In *Int. Conf. Comp. Vis. (ICCV)*, 2009.

[19] J. Lellmann, J. Kappes, J. Yuan, F. Becker, and C. Schnörr. Convex multiclass image labeling by simplex-constrained total variation. Technical report, HCI, IWR, University of Heidelberg, 2008.

[20] P. K. Lubor Ladicky, Chris Russell and P. Torr. Graph cut based inference with co-occurrence statistics. In *Proceedings of ECCV*, 2010.

[21] K. McGuinness and N. O'Connor. A comparative evaluation of interactive segmentation algorithms. *Pattern Recognition*, 43(1):434–444, 2010.

[22] C. Michelot. A finite algorithm for finding the projection of a point onto the canonical simplex of r^n. *Journal of Optimization Theory and Applications*, 50(1):195–200, 1986.

[23] D. Mumford and J. Shah. Optimal approximation by piecewise smooth functions and associated variational problems. *Comm. Pure Appl. Math.*, 42:577–685, 1989.

[24] C. Nieuwenhuis, B. Berkels, M. Rumpf, and D. Cremers. Interactive motion segmentation. In *Pattern Recognition (Proc. DAGM)*, volume 6376, pages 483–492, 2010.

[25] C. Nieuwenhuis, E. Töppe, and D. Cremers. Space-varying color distributions for interactive multiregion segmentation: Discrete versus continuous approaches. In *Proceedings of Energy Minimization Methods in Computer Vision and Pattern Recognition (EMMCVPR)*, 2011.

[26] T. Pock and A. Chambolle. Diagonal preconditioning for first order primal-dual algorithms in convex optimization. In *IEEE Int. Conf. on Computer Vision*, 2011.

[27] T. Pock, A. Chambolle, H. Bischof, and D. Cremers. A convex relaxation approach for computing minimal partitions. In *IEEE Conference on Computer Vision and Pattern Recognition (CVPR)*, 2009.

[28] T. Pock, D. Cremers, H. Bischof, and A. Chambolle. An algorithm for minimizing the piecewise smooth Mumford-Shah functional. In *IEEE Int. Conf. on Computer Vision*, Kyoto, Japan, 2009.

[29] R. B. Potts. Some generalized order-disorder transformations. *Proc. Camb. Phil. Soc.*, 48:106–109, 1952.

[30] C. Rhemann, C. Rother, and M. Gelautz. Improving color modeling for alpha matting. In *British Machine Vision Conference (BMVC)*, 2008.

[31] F. Rosenblatt. Remarks on some nonparametric estimates of a density function. *Annals of Mathematical Statistics*, 27:832–837, 1956.

[32] C. Rother, V. Kolmogorov, and A. Blake. Grab-cut: interactive foreground segmentation using iterated graph cuts. *ACM Transactions on Graphics*, 23(3):309–314, 2004.

[33] L. Rudin, S. Osher, and E. Fatemi. Nonlinear Total Variation based noise removal algorithms. *Physica D*, 60:259–268, 1992.

[34] J. Santner. *Interactive Multi-label segmentation*. PhD thesis, University of Graz, 2010.

[35] J. Santner, T. Pock, and H. Bischof. Interactive multi-label segmentation. In *Proceed. of the Asian Conference on Computer Vision (ACCV)*, 2010.

[36] B. W. Silverman. *Density estimation for statistics and data analysis*. Chapman and Hall, London, 1992.

[37] Y. Tai, J. Jia, and C. Tang. Soft color segmentation and its applications. *IEEE Trans. on Patt. Anal. and Mach. Intell.*, 29(9):1520–1537, 2007.

[38] M. Taron, N. Paragios, and M.-P. Jolly. Border detection on short axis echocardiographic views using an ellipse driven region-based framework. In *MICCAI*, volume 3216, pages 443–450. Springer, 2004.

[39] M. Unger, T. Pock, W. Trobin, D. Cremers, and H. Bischof. TVSeg - interactive total variation based image segmentation. In *Proceedings of the 19th British Machine Vision Conference*, 2008.

[40] J. Wang and M. Cohen. Optimized color sampling for robust matting. In *Computer Vision and Pattern Recognition*, pages 1 –8, 2007.

[41] J. Yuan and Y. Boykov. TV-based image segmentation with label cost prior. In *Proceedings of the British Machine Vision Conference*, 2010.

[42] C. Zach, D. Gallup, J.-M. Frahm, and M. Niethammer. Fast global labeling for real-time stereo using multiple plane sweeps. In *Vision, Modeling and Visualization Workshop VMV 2008*, 2008.

Claudia Nieuwenhuis received a MS (Diplom) in Computer Science from the Technical University of Ilmenau in 2006 and a MS (Diplom) in Mathematics from the University of Hagen in 2008. In 2009 she obtained a PhD in Computer Science from the University of Heidelberg. Between 2003 and 2006 she worked for a year and a half at Siemens Corporate Research in Princeton, USA, and at the Fraunhofer Center for Advanced Media Technology in Singapore. After her PhD she stayed as a postdoctoral researcher with Prof. Rudolf Mester at the University of Frankfurt. Since October 2009 she has been with the Computer Vision and Pattern Recognition group at the Technical University of Munich headed by Prof. Daniel Cremers.

Daniel Cremers received a MS (Diplom) in Theoretical Physics (1997) from the University of Heidelberg and a PhD in Computer Science (2002) from the University of Mannheim, Germany. Subsequently he spent two years as a postdoctoral researcher at the UCLA and one year as a permanent researcher at Siemens Corporate Research in Princeton. From 2005 until 2009 Prof. Cremers headed the Computer Vision Group at the University of Bonn, Germany. Since 2009 he is full professor for computer science and mathematics at the TU München. He received several awards, including the *Best Paper of the Year 2003* by the Pattern Recognition Society, the *Olympus Award 2004*, and the *2005 UCLA Chancellor's Award*.